Reconstruction of Nonuniformly Sampled Bandlimited Signals Using a Differentiator–Multiplier Cascade

Stefan Tertinek and Christian Vogel, *Member, IEEE*

***Abstract*—This paper considers the problem of reconstructing a bandlimited signal from its nonuniform samples. Based on a discrete-time equivalent model for nonuniform sampling, we propose the differentiator–multiplier cascade, a multistage reconstruction system that recovers the uniform samples from the nonuniform samples. Rather than using optimally designed reconstruction filters, the system improves the reconstruction performance by cascading stages of linear-phase finite impulse response (FIR) filters and time-varying multipliers. Because the FIR filters are designed as differentiators, the system works for the general nonuniform sampling case and is not limited to periodic nonuniform sampling. To evaluate the reconstruction performance for a sinusoidal input signal, we derive the signal-to-noise-ratio at the output of each stage for the two-periodic and the general nonuniform sampling case. The main advantage of the system is that once the differentiators have been designed, they are implemented with fixed multipliers, and only some general multipliers have to be adapted when the sampling pattern changes; this reduces implementation costs substantially, especially in an application like time-interleaved analog-to-digital converters (TI-ADCs) where the timing mismatches among the ADCs may change during operation.**

***Index Terms*—Discrete-time differentiator, Farrow structure, nonuniform sampling, Taylor series expansion, time-interleaved analog-to-digital converter (TI-ADC), time-varying multiplier.**

I. Introduction

In digital signal processing, the standard method for converting a continuous-time signal into a discrete-time signal is uniform sampling where samples are taken at uniform time instances. If the continuous-time signal is bandlimited and the sampling rate is at least equal to the Nyquist rate, then the original signal can be uniquely reconstructed from these uniform samples by ideal low-pass interpolation [1]. In many practical applications, sampling occurs at nonuniform time instances [2]. Similar to uniform sampling, if the average sampling rate is at least equal to the Nyquist rate, then the bandlimited continuous-time signal is uniquely determined by these nonuniform samples [3]. Although direct reconstruction using continuous-time interpolation functions is, in principle, possible [4], [5], a practical implementation of these functions with high precision is computationally difficult. Alternatively, iterative reconstruction methods can be used [2], [6], but they have potential convergence problems and are computationally demanding. To benefit from an all-digital implementation, the most efficient reconstruction method is to recover the uniform samples from the nonuniform samples in the digital domain. A practical digital reconstruction technique is to use time-varying discrete-time filters, which are automatically obtained by sampling and truncating the ideal continuous-time interpolation functions. To circumvent the problems associated with truncation, the authors in [7] assumed a slight oversampling and developed least-squares and minimax design procedures based on a time-frequency function. Although the obtained reconstruction filters have minimum order, a new design is required for each sampling instance such that online design increases the implementation costs significantly. However, for M-periodic nonuniform sampling, where the nonuniform sampling instances form an M-periodic pattern, the design problem can be posed as one of a filter bank. The obtained reconstruction filters approximating the ideal ones in [8] have orders less than those proposed in [9] and [10]. Reconstructing periodic nonuniformly sampled signals is of practical importance in time-interleaved analog-to-digital converters (TI-ADCs) where timing mismatches among the ADCs give rise to the recurrent sampling pattern [11]. Although these mismatches are usually assumed to be known, estimating them is also an issue [12], [13]. More importantly, temperature and aging affect the mismatches, causing the sampling pattern to change during operation [14]. To avoid online filter redesign in that case, a digital fractional delay filter bank was developed in [15] for moderately oversampled signals. Applying their framework developed in [7], the same authors used polynomial impulse response time-varying finite-impulse response (FIR) filters for reconstruction in the two-periodic case [16], [17]. Although the obtained filter orders are higher than those in [7], the implementation costs are kept low in that the filters are designed offline and are implemented with fixed multipliers; only a few general multipliers need to be adapted when the sampling pattern changes. Yet, using multivariate polynomials for the M-periodic case significantly increases the design and

Manuscript received July 7, 2007; revised December 5, 2007. First published February 8, 2008; current version published September 17, 2008. The work of C. Vogel was supported by the Austrian Science Fund FWF's Erwin Schrödinger Fellowship J2709-N20. This paper was recommended by Associate Editor B. C. Levy.

S. Tertinek was with the Signal Processing and Speech Communication Laboratory, Graz University of Technology, A-8010 Graz, Austria. He is now with the Circuits and Systems Group, University College Dublin, Dublin 4, Ireland (e-mail: stertinek@ee.ucd.ie).

C. Vogel was with the Signal Processing and Speech Communication Laboratory, Graz University of Technology, A-8010 Graz, Austria. He is now with the Department of Information Technology and Electrical Engineering, ETH Zurich, CH-8092 Zurich, Switzerland (e-mail: c.vogel@ieee.org).

Digital Object Identifier 10.1109/TCSI.2008.918267

implementation complexity, such that these filters with the current design techniques may only be used for small time errors and small M [18].

A. Contribution of this Paper and Relation to Other Work

To make the M-variate polynomial impulse response filter approach generally applicable, it was pointed out in [17] that a scheme with a reduced number of subfilters and systematic design techniques for the general case are required. In our previous work [19], we derived one such special scheme consisting of an FIR filter designed as differentiator and a time-varying multiplier. The main advantage of that system is that designing the optimal reconstruction filters reduces to designing a simple FIR differentiator. Because this design is independent of M, the system can, in fact, be used for any number of M and does not face the design problems reported for the M-variate polynomial impulse response filters in [18]. The simple filter design comes with the drawback that the system is neither optimal in any sense nor can it achieve an arbitrarily small reconstruction error, contrary to the polynomial impulse response filters.

The main contribution of this paper is to extend the system in [19] and propose the differentiator–multiplier cascade (DMC), an all-digital reconstruction system that improves the reconstruction performance by cascading several stages. Because each stage consists only of linear-phase FIR filters designed as differentiators and time-varying multipliers, the DMC can also be used for the general nonuniform sampling case. Moreover, the implementation costs are reduced because once the FIR differentiators have been designed, they are implemented with fixed multipliers, and only a few general multipliers need to be adapted when the sampling pattern changes over time.

The second contribution is to introduce a reconstruction principle that is different from the (mostly filter bank based) methods proposed so far. Based on our work in [19] where we considered canceling an error spectrum in the frequency domain, we show in Section II how to perform error canceling in the discrete-time domain. For this purpose, we develop in Section III a discrete-time equivalent model that represents the nonuniform samples as the sum of the uniform samples and error samples accounting for the amplitude error due to nonuniform sampling. Based on this equivalent model, the idea is to cancel the error samples by first reconstructing them and then subtracting their reconstructed version from the nonuniform samples. This principle leads in Section IV and Section V to the proposed DMC that cancels the error samples using a cascade of reconstruction stages. In Section VI, we show how redrawing the DMC leads to a system with a reduced overall delay, but at the cost of a slightly worse reconstruction performance. To evaluate the reconstruction performance of the system for a sinusoidal input signal, we derive in Section V the theoretical signal-to-noise ratio (SNR) at the output of each stage for the cases $M = 2$ and large M. Section VIII deals with the practical implementation of the DMC and considers some implementation issues. Simulation results in Section IX illustrate the reconstruction performance and confirm the derived SNR expressions. Finally, Section X gives the conclusions.

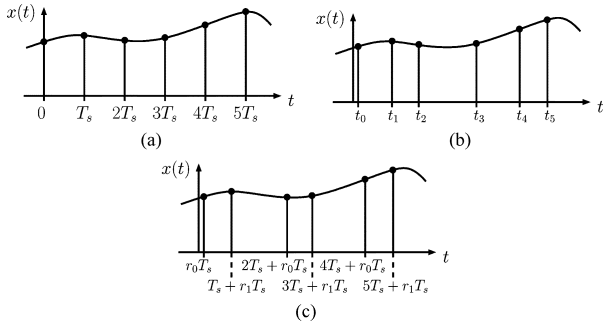

Fig. 1. (a) Uniform sampling, (b) nonuniform sampling, and (c) two-periodic nonuniform sampling.

II. Nonuniform Sampling and Proposed Reconstruction Principle

Uniform sampling refers to taking periodically spaced samples from a continuous-time signal $x(t)$, as shown in Fig. 1(a). Denoting the sampling period as T_s, uniform sampling produces the sequence

$$x[n] = x(nT_s) \tag{1}$$

which is referred to as the uniform sequence. We assume throughout this paper that $x(t)$ is bandlimited, i.e., its Fourier transform satisfies

$$X(j\Omega) = 0, \quad |\Omega| \geq W, \qquad W \leq \pi/T_s \tag{2}$$

where W is the signal bandwidth. Because (2) ensures that sampling occurs at least at the Nyquist rate, the original signal $x(t)$ can be recovered from the uniform sequence $x[n]$ [1].

Nonuniform sampling, by contrast, refers to taking samples at arbitrary time instances t_n and produces the sequence $y[n] = x(t_n)$. In this paper, we assume that the time instances t_n deviate from the uniform sampling points nT_s according to

$$t_n = nT_s + r_nT_s \tag{3}$$

as shown in Fig. 1(b). The time errors r_n, given as fraction of the average sampling period T_s, determine the deviation of the nonuniform from the uniform sampling instances and are assumed to be known. With (3), the sequence obtained by nonuniform sampling becomes

$$y[n] = x(nT_s + r_nT_s) \tag{4}$$

which is referred to as the nonuniform sequence. When the time errors r_n are periodic with period M, i.e., $r_n = r_{n+M}$, we have the M-periodic nonuniform sampling case, which is depicted in Fig. 1(c) for $M = 2$. In TI-ADCs, for example, this periodic sampling pattern is caused by timing mismatches among the ADCs. We further assume that the time errors r_n are less than some tenth, a typical range for such an application [20].

The goal of reconstruction in the digital domain is to recover the uniform sequence $x[n]$ in (1) from the nonuniform sequence $y[n]$ in (4). To this end, we propose the reconstruction principle shown in Fig. 2. The model part corresponds to the discrete-time

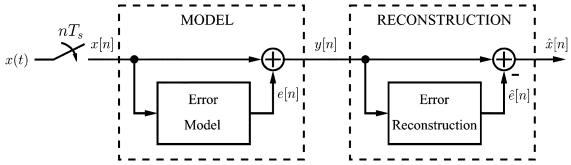

Fig. 2. Proposed reconstruction principle consisting of a model part and a reconstruction part.

equivalent model for nonuniform sampling that will be derived in Section III. This model represents the nonuniform sequence $y[n]$ as the sum of the uniform sequence $x[n]$ and an error sequence $e[n]$; i.e.,

$$y[n] = x[n] + e[n] \tag{5}$$

where $e[n]$ accounts for the amplitude error introduced by nonuniform sampling. Given the model in (5), the main idea is to reconstruct $x[n]$ from $y[n]$ by canceling $e[n]$. As the reconstruction part in the figure shows, this requires two steps: reconstructing the error $e[n]$ and subtracting the reconstructed error $\hat{e}[n]$ from $y[n]$. This subtraction results in the reconstructed uniform sequence

$$\hat{x}[n] = y[n] - \hat{e}[n] \tag{6}$$

which will be equal to $x[n]$ if we can perfectly reconstruct $e[n]$, i.e., if $\hat{e}[n] = e[n]$. Based on the reconstruction principle in Fig. 2, we will start with deriving the discrete-time equivalent model in the next section and continue with developing the reconstruction system in later sections.

III. Discrete-Time Equivalent Model for Nonuniform Sampling of Bandlimited Signals

In this section, we derive a discrete-time equivalent model for sampling a bandlimited continuous-time signal $x(t)$ at the nonuniform time instances in (3). We use the term equivalent model because nonuniform sampling of $x(t)$ turns out to be equivalent to uniform sampling of both $x(t)$ and all of its weighted derivatives. To derive the model, consider the kth sampling instance shown in Fig. 3. An ideal sampling device samples $x(t)$ at the uniform time instance kT_s, leading to the correct sample value $x(kT_s)$. However, nonidealities determined by the time error r_k cause sampling to occur at the nonuniform time instance $kT_s + r_kT_s$, resulting in the incorrect sample value $x(kT_s + r_kT_s)$. Now, the basic idea is to model $x(kT_s + r_kT_s)$ as the sum of $x(kT_s)$ and the error sample $e(kT_s)$ that accounts for the amplitude error due to nonuniform sampling. Because we assume that r_k is sufficiently small and that $x(t)$ is bandlimited, the resulting small amplitude error suggests a local signal representation. Therefore, we expand $x(t)$ into a Taylor series about the uniform sampling instance kT_s. In general, assuming that all derivatives of $x(t)$ exist, the Taylor series expansion of the signal about the time instance t_0 is [21]

$$x(t_0 + \Delta t) = x(t_0) + \sum_{l=1}^{\infty} \frac{1}{l!} \Delta t^l x^{(l)}(t_0) \tag{7}$$

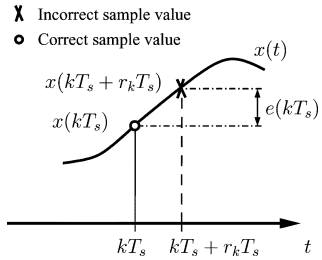

Fig. 3. Sampling a continuous-time signal $x(t)$ at the nonuniform time instance $kT_s + r_kT_s$, rather than at the uniform time instance kT_s, introduces the amplitude error $e(kT_s)$.

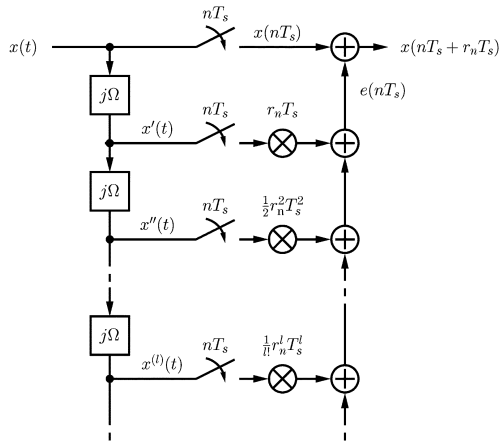

Fig. 4. Equivalent model for nonuniform sampling of a continuous-time signal $x(t)$ having all derivatives.

where Δt determines the deviation from t_0, and $x^{(l)}(t)$ denotes the lth derivative of $x(t)$. Applying this relation to Fig. 3 and considering the Taylor series expansion about all sampling instances, we set $t_0 = nT_s$ and $\Delta t = r_nT_s$ and can express (7) as

$$x(nT_s + r_nT_s) = x(nT_s) + e(nT_s) \tag{8}$$

where the amplitude error is

$$e(nT_s) = \sum_{l=1}^{\infty} \frac{1}{l!} r_n^l T_s^l x^{(l)}(nT_s). \tag{9}$$

Equations (8) and (9) constitute the equivalent model for nonuniform sampling depicted in Fig. 4. The model represents the nonuniform samples $x(nT_s + r_nT_s)$ as the sum of the uniform samples $x(nT_s)$ and the error samples $e(nT_s)$, which are the weighted sum of uniform samples of all derivatives of $x(t)$. In particular, the figure shows that the lth term in this sum consists of $x^{(l)}(t)$, which is produced by a chain of l continuous-time differentiators with frequency response $j\Omega$, being sampled at nT_s and weighted by $r_n^lT_s^l/l!$.

Assuming that $x(t)$ is bandlimited according to (2), we can convert Fig. 4 into the discrete-time equivalent model shown in Fig. 5. The bandlimitedness ensures that $x^{(l)}(t)$ exists for all l and allows us to change the order of differentiation and sampling. To be specific, we can replace each continuous-time differentiator with frequency response $j\Omega$ by an equivalent discrete-time system with frequency response $j\omega/T_s$, where $-\pi \leq \omega < \pi$ [1]. Since generating the lth derivative using a chain of

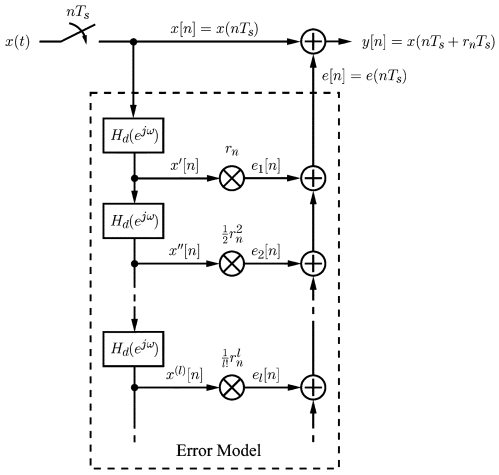

Fig. 5. Discrete-time equivalent model for nonuniform sampling of a bandlimited continuous-time signal $x(t)$.

l such systems introduces the factor $1/T_s^l$, the factor T_s^l in (9) will be canceled. Therefore, inserting (9) into (8) and using (1), (4) and $e[n] = e(nT_s)$, we can write (5) as

$$y[n] = x[n] + \sum_{l=1}^{\infty} e_l[n] \tag{10}$$

where

$$e_l[n] = \frac{1}{l!} r_n^l x^{(l)}[n]. \tag{11}$$

Similar to the model in Fig. 4, $x^{(l)}[n]$ in Fig. 5 is produced by a chain of l ideal discrete-time differentiators with frequency response [1]

$$H_d(e^{j\omega}) = j\omega, \quad -\pi \le \omega < \pi \tag{12}$$

which is equivalent to write $x^{(l)}[n] = (h_d * \cdots * h_d * x)[n]$, where the impulse response of the differentiator, $h_d[n]$, is convolved with itself $(l-1)$-times. In view of this, $z^{(l)}[n]$ denotes l-times (discrete-time) differentiating an arbitrary sequence $z[n]$. For example, $y'[n] = h_d[n] * y[n]$ refers to differentiating the sequence $y[n]$ in (10), which is equivalent to sampling the derivative of a corresponding bandlimited continuous-time signal $y(t)$. Furthermore, we refer to (11) as the lth-order error or, equivalently, the error of order $O(r_n^l)$; this notation indicates that higher order errors contribute less to the total error $e[n]$ than lower order errors because of the smaller weighting factor $r_n^l/l!$. For example, the second-order error $e_2[n] = (1/2)r_n^2 x''[n]$ (or error of order $O(r_n^2)$) contributes less to the total error $e[n]$ than the first-order error $e_1[n] = r_n x'[n]$ (or error of order $O(r_n)$). Note further that for vanishing r_n, the model in Fig. 5 reduces to the uniform sampling process in (1). Moreover, if we consider only the first L terms in the model, then the approximation is equal to a Farrow structure whose subfilters have frequency responses $H_d^l(e^{j\omega})/l!$, for $l = 0, 1, \ldots, L-1$ [22]. This approximation was used in [23] to transform the design problem of a fractional delay filter into one of a first-order differentiator, but the derivation of the subfilters (differentiators) in the Farrow structure was given in the frequency domain. In [24], the Taylor series expansion in (7) about $t_0 = 0$ was interpreted as an infinite filter bank, where the analysis filters have frequency responses $(j\omega)^k$ and the synthesis filters have impulse responses $t^k/k!$, for $0 \le k \le \infty$. Contrary to these approaches, we will use the discrete-time equivalent model to derive a reconstruction method for nonuniformly sampled signals in the following sections.

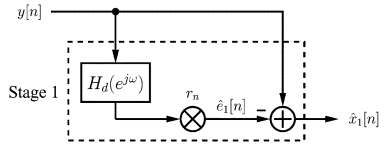

Fig. 6. First stage consisting of a discrete-time differentiator $H_d(e^{j\omega})$ and a time-varying multiplier r_n.

IV. First-Order Error Canceling Using A Discrete-Time Differentiator and A Time-Varying Multiplier

Having introduced the model part of the reconstruction principle in Fig. 2, we now consider the reconstruction part and derive the reconstruction system in Fig. 6. We refer to this system as the first stage because it will be the first stage of the DMC developed in Section V. In our previous work [19], we obtained this system by canceling an error spectrum in the frequency domain. The derivation was simplified by considering only the two-periodic nonuniform sampling case, and it was pointed out that the system can be adapted for the M-periodic case by using an M-periodic time-varying multiplier. By contrast, the derivation in this section is given in the time domain and is solely based on the reconstruction principle in Fig. 2. Since the time errors will not be assumed periodic, it will become clear that the reconstruction system also works for the general nonuniform sampling case.

We begin by recalling that, given the model $y[n] = x[n] + e[n]$, our goal is to cancel the error $e[n]$ by subtracting its reconstructed version $\hat{e}[n]$ from $y[n]$. Comparing (5) and (10) shows that

$$e[n] = \sum_{l=1}^{\infty} e_l[n]. \tag{13}$$

Thus, to cancel $e[n]$, we cancel each error term $e_l[n]$ by subtracting its reconstructed version $\hat{e}_l[n]$ from $y[n]$. To find $\hat{e}_l[n]$, observe from (11) that $e_l[n]$ could be produced from $x[n]$ using two basic operations: discrete-time differentiation and time-varying multiplication. To illustrate the error reconstruction in the ideal case, let us assume that we knew $x[n]$. We could then apply these two operations to $x[n]$ to exactly reconstruct each $e_l[n]$. In particular, differentiating $x[n]$ and multiplying by r_n would give $\hat{e}_1[n] = r_n x'[n]$, which is equal to the first-order error $e_1[n]$. In a similar manner, we could also reconstruct the higher order errors. Knowing $x[n]$, however, would not require a reconstruction system, and the only available sequence is $y[n]$. But since $y[n]$ also consists of $x[n]$ according to (10), we can reconstruct each $e_l[n]$ by applying the same two operations to $y[n]$, and thereby to $x[n]$. Because we saw in Section III that higher order errors contribute less to the total error $e[n]$, we

begin with canceling $e_1[n]$. To simplify the error analysis, we approximate $y[n]$ using the first two error terms in (10); i.e.,

$$y[n] \approx x[n] + e_1[n] + e_2[n] \tag{14}$$

where $e_2[n]$ will be used for error evaluation. We now apply the two-step approach described above: error reconstruction and subtraction from $y[n]$.

In the first step, we reconstruct $e_1[n]$ by differentiating $y[n]$ and multiplying by r_n; thus, we obtain the reconstructed first-order error through

$$\hat{e}_1[n] = r_n y'[n] \tag{15}$$

which can be approximated with (14) by

$$\hat{e}_1[n] \approx r_n x'[n] + r_n e_1'[n] + r_n e_2'[n]. \tag{16}$$

It should be emphasized that approximating $y[n]$ in (14), and thus $\hat{e}_1[n]$ in (16), only serves to simplify the SNR derivation in Section VII, whereas the actual reconstruction step in (15) is performed on $y[n]$ itself, including all error terms. The approximation in (16) also shows that the step in (15) not only reconstructs the error $e_1[n] = r_n x'[n]$ but also introduces two additional errors; the first error $r_n e_1'[n]$ is of order $O(r_n^2)$ because it is produced by multiplying the error $e_1'[n]$ of order $O(r_n)$ by r_n; the second error $r_n e_2'[n]$ is of order $O(r_n^3)$ because it is produced by multiplying the error $e_2'[n]$ of order $O(r_n^2)$ by r_n. Analyzing additionally introduced errors with respect to their order will allow us to neglect some of them. In fact, we will see in Section VII that for the ith DMC stage, errors up to order $O(r_n^{i+1})$ are sufficient to determine the SNR and higher order errors can be neglected. The simulation results in Section IX will confirm this conclusion.

In the second step of our approach, we cancel $e_1[n]$ in (14) by subtracting its reconstructed version $\hat{e}_1[n]$ found in (15). This subtraction gives the reconstructed uniform sequence

$$\hat{x}_1[n] = y[n] - \hat{e}_1[n] \tag{17}$$

which corresponds to the output of the first stage. Fig. 6 depicts the first stage of the reconstruction system given by (15) and (17). The discrete-time differentiator $H_d(e^{j\omega})$ followed by the time-varying multiplier r_n produces the reconstructed first-order error $\hat{e}_1[n]$ which is subtracted from $y[n]$ to cancel $e_1[n]$. The resulting reconstructed uniform sequence in (17) can be approximated with (14) and (16) by

$$\hat{x}_1[n] \approx x[n] - r_n e_1'[n] + e_2[n] \tag{18}$$

where errors of order $O(r_n^3)$ and higher have been neglected. Equation (18) shows that $e_1[n]$ has been canceled, but at the cost of the additionally introduced error $r_n e_1'[n]$. Besides $e_2[n]$, which is inherent in our model for $y[n]$, this additional error limits the reconstruction performance of the first stage by introducing a performance floor [19]. Moreover, large time errors r_n, which occur in bunched sampling [9], lead to a poor reconstruction performance because $r_n e_1'[n]$ may become larger than the error $e_1[n]$ actually being canceled. On the other hand, the polynomial impulse response time-varying FIR filters introduced in [16] and [18], of which the first stage in Fig. 6 is a special case [19], can be designed to achieve optimal overall performance in the least-squares and minimax sense for an arbitrarily small reconstruction error. As M increases, however, the filter design becomes increasingly complex, whereas the first stage still requires only the design of a differentiator, independent of M. This significant advantage in the filter design, but the poor reconstruction performance, motivates the extension of the first stage to improve the reconstruction quality, as will be shown in the next section.

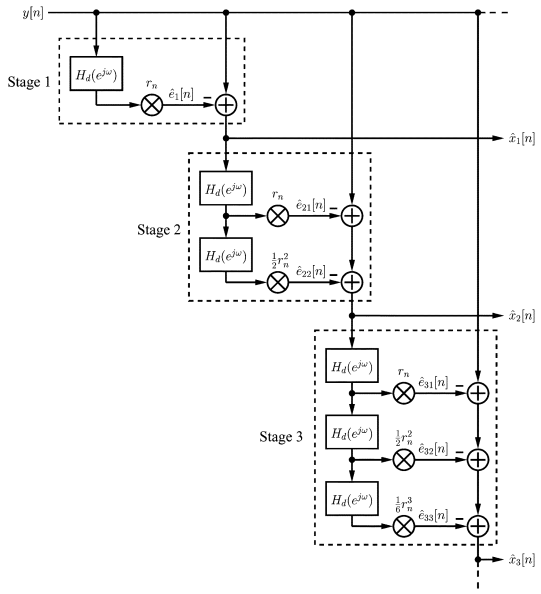

Fig. 7. Proposed DMC. Each stage consists only of discrete-time differentiators $H_d(e^{j\omega})$ and time-varying multipliers.

V. DMC for Canceling Higher Order Errors

To extend the first stage, we derive in this section the DMC in Fig. 7, a multistage reconstruction system using only discrete-time differentiators and time-varying multipliers. Compared with the first stage in Fig. 6, the DMC improves the reconstruction quality by also canceling the higher order errors $e_2[n]$, $e_3[n]$, and so on. Generally speaking, the difficulty in extending the first stage is the additionally introduced error. In particular, we saw in (18) that using $y[n]$ to cancel $e_1[n]$ introduces the error $r_n e_1'[n]$. If we extended the first stage by using $y[n]$ to cancel only the second-order error $e_2[n]$ (or even higher order errors), then the reconstruction quality would only slightly improve because the error $r_n e_1'[n]$ would still be left. Therefore, an obvious idea is to use $y[n]$ to cancel both $e_2[n]$ and $r_n e_1'[n]$. The problem with this approach is that reconstructing the additionally introduced errors in each stage becomes increasingly complex.

The idea leading to the DMC is based on the fact that the output of the first stage, $\hat{x}_1[n]$, is closer to $x[n]$ than $y[n]$, where closer is defined in terms of the SNR. Hence, rather than $y[n]$, we use $\hat{x}_1[n]$ for further error reconstruction. In particular, we

use $\hat{x}_1[n]$ to cancel $e_1[n]$ and $e_2[n]$ simultaneously. To this end, we approximate $y[n]$ using the first three error terms in (10); i.e.,

$$y[n] \approx x[n] + e_1[n] + e_2[n] + e_3[n] \tag{19}$$

where $e_1[n] = r_n x'[n]$ and $e_2[n] = (1/2) r_n^2 x''[n]$ will be canceled and $e_3[n]$ will be used for error evaluation. Applying again the two-step approach from before, we first reconstruct $e_1[n]$ and $e_2[n]$ using $\hat{x}_1[n]$ by

$$\hat{e}_{21}[n] = r_n \hat{x}_1'[n] \tag{20}$$

$$\hat{e}_{22}[n] = \frac{1}{2} r_n^2 \hat{x}_1''[n] \tag{21}$$

respectively, which can be approximated with (18) and neglecting terms of order $O(r_n^4)$ and higher by

$$\hat{e}_{21}[n] \approx r_n x'[n] - r_n \left(r_n e_1'[n]\right)' + r_n e_2'[n] \tag{22}$$

$$\hat{e}_{22}[n] \approx \frac{1}{2} r_n^2 x''[n]. \tag{23}$$

Then, we cancel $e_1[n]$ and $e_2[n]$ by subtracting their reconstructed versions $\hat{e}_{21}[n]$ and $\hat{e}_{22}[n]$, respectively, from $y[n]$. This subtraction gives the reconstructed uniform sequence

$$\hat{x}_2[n] = y[n] - \hat{e}_{21}[n] - \hat{e}_{22}[n] \tag{24}$$

which corresponds to the output of the second stage. Fig. 7 shows the second stage given by (20), (21) and (24). The output of the first stage, $\hat{x}_1[n]$, runs through two differentiators $H_d(e^{j\omega})$ to produce $\hat{x}_1'[n]$ and $\hat{x}_1''[n]$. These two sequences are multiplied by r_n and $(1/2) r_n^2$ to generate the reconstructed errors $\hat{e}_{21}[n]$ and $\hat{e}_{22}[n]$, respectively. Using (19), (22) and (23), we can approximate (24) by

$$\hat{x}_2[n] \approx x[n] + r_n \left(r_n e_1'[n]\right)' - r_n e_2'[n] + e_3[n]. \tag{25}$$

Similar to the first stage, (25) shows that $e_1[n]$ and $e_2[n]$ in (19) have been canceled, but at the cost of the two additionally introduced errors $r_n(r_n e_1'[n])'$ and $r_n e_2'[n]$; they are caused by the errors $r_n e_1'[n]$ and $e_2[n]$ of the first stage propagating through the first-order branch ($H_d(e^{j\omega})$ followed by r_n) of the second stage. By contrast, the same two errors propagating through the second-order branch do not introduce any significant error terms. This will be the key observation in Section VI to redraw the DMC and derive a reconstruction system with reduced delay.

We can further improve the reconstruction quality by adding a third stage. Using $\hat{x}_2[n]$ to cancel $e_1[n]$, $e_2[n]$ and $e_3[n]$ simultaneously, we approximate $y[n]$ using the first four error terms in (10); i.e.,

$$y[n] \approx x[n] + e_1[n] + e_2[n] + e_3[n] + e_4[n] \tag{26}$$

where $e_4[n]$ will be used for error evaluation. To cancel $e_1[n]$, $e_2[n]$ and $e_3[n]$, we first reconstruct them using $\hat{x}_2[n]$ by

$$\hat{e}_{31}[n] = r_n \hat{x}_2'[n] \tag{27}$$

$$\hat{e}_{32}[n] = \frac{1}{2} r_n^2 \hat{x}_2''[n] \tag{28}$$

$$\hat{e}_{33}[n] = \frac{1}{6} r_n^3 \hat{x}_2'''[n]. \tag{29}$$

Then, we subtract these reconstructed errors from $y[n]$ and get the reconstructed uniform sequence

$$\hat{x}_3[n] = y[n] - \hat{e}_{31}[n] - \hat{e}_{32}[n] - \hat{e}_{33}[n] \tag{30}$$

which corresponds to the output of the third stage. Fig. 7 shows the third stage given by (27)–(30). The output of the second stage, $\hat{x}_2[n]$, runs through three branches to produce $\hat{e}_{31}[n]$, $\hat{e}_{32}[n]$ and $\hat{e}_{33}[n]$, which are subtracted from $y[n]$ to cancel $e_1[n]$, $e_2[n]$ and $e_3[n]$, respectively. Inserting (25) into (27)–(29), and the result with (26) into (30), we can approximate $\hat{x}_3[n]$ by

$$\hat{x}_3[n] \approx x[n] - r_n \left(r_n \left(r_n e_1'[n]\right)'\right)' + r_n \left(r_n e_2'[n]\right)' - r_n e_3'[n] + e_4[n] \tag{31}$$

where errors of order $O(r_n^5)$ and higher have been neglected. Similar to the first and second stage, the three additionally introduced errors in (31) are caused by the errors $r_n(r_n e_1'[n])'$, $r_n e_2'[n]$ and $e_3[n]$ of the second stage propagating through the first-order branch of the third stage.

To simplify the SNR derivation in Section VII, we generalize this error propagation through each stage. Defining the remaining error of the ith stage as

$$\bar{e}_i[n] = \hat{x}_i[n] - x[n] \tag{32}$$

where the stage number $i = 1, 2, 3$, we can approximate the remaining error of the first stage with (18) by

$$\begin{aligned} \bar{e}_1[n] &\approx e_2[n] - r_n e_1'[n] \\ &= e_2[n] - r_n \bar{e}_0'[n] \end{aligned} \tag{33}$$

where $\bar{e}_0[n] := e_1[n]$. Similarly, we can approximate the remaining error of the second stage with (25) by

$$\begin{aligned} \bar{e}_2[n] &\approx e_3[n] - r_n e_2'[n] + r_n \left(r_n e_1'[n]\right)' \\ &= e_3[n] - r_n \bar{e}_1'[n] \end{aligned} \tag{34}$$

and the remaining error of the third stage with (31) by

$$\begin{aligned} \bar{e}_3[n] &\approx e_4[n] - r_n e_3'[n] + r_n \left(r_n e_2'[n]\right)' - r_n \left(r_n \left(r_n e_1'[n]\right)'\right)' \\ &= e_4[n] - r_n \bar{e}_2'[n]. \end{aligned} \tag{35}$$

From (33)–(35), it can be seen that the remaining error of the ith stage may be expressed as

$$\bar{e}_i[n] \approx e_{i+1}[n] - r_n \bar{e}_{i-1}'[n]. \tag{36}$$

As depicted in Fig. 8, $\bar{e}_i[n]$ can be approximated by two terms: the error $e_{i+1}[n]$, which accounts for approximating $y[n]$ in the ith stage, and the additionally introduced error $r_n \bar{e}_{i-1}'[n]$, which corresponds to the remaining error of the $(i-1)$th stage, $\bar{e}_{i-1}[n]$, propagating through the first-order branch shown in the figure. Note that (36) only consists of errors up to order $O(r_n^{i+1})$ and higher order errors have been neglected. We will see that this gives a reasonable approximation for each stage because the derived SNR based on (36) agrees with the simulation results in Section IX. Simulation results also showed that additional stages improve the reconstruction quality further

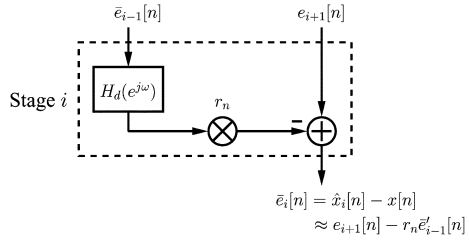

Fig. 8. Approximating the remaining error of the ith stage, $\bar{e}_i[n]$, by (36).

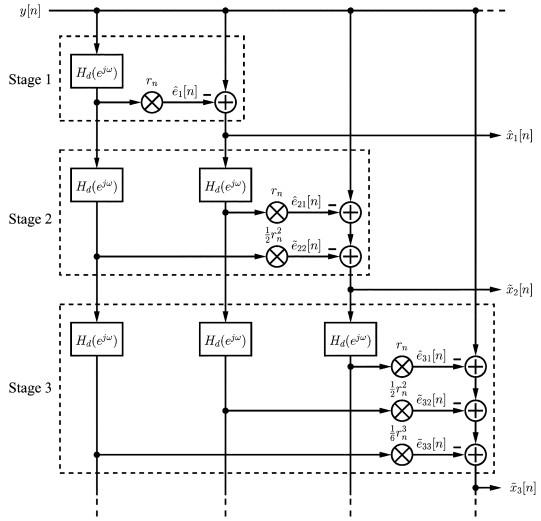

Fig. 9. DMC-RD.

and are needed especially for large time errors. The overall complexity of the reconstruction system, however, increases considerably.

This section concludes by considering the total delay of the DMC. In Section IX, we will see that a practical implementation of the system requires the design of a linear-phase FIR filter whose frequency response approximates the frequency response of the ideal differentiator. Assuming that this FIR filter has a delay of D, the delay of the ith stage in Fig. 7 is iD because of the chain of i differentiators. Therefore, the total delay of the DMC with m stages is

$$D_m^{\mathrm{DMC}} = \sum_{i=1}^{m} iD = \frac{1}{2}m(m+1)D \tag{37}$$

where $m = 1, 2, 3$ in our case. For $D = 16$, for example, the total delay with three stages is $D_3^{\mathrm{DMC}} = 96$ which is larger than a delay of D for a filter bank based reconstruction system. To use the DMC in an application requiring a low system delay, we will show in the next section how redrawing the DMC leads to a reconstruction system with reduced total delay.

VI. Reducing Delay of DMC

The DMC with reduced delay (DMC-RD) derived in this section is shown in Fig. 9. The main difference to the DMC in Fig. 7 is that the second stage uses not only $\hat{x}_1[n]$ for error reconstruction but also $y[n]$. Likewise, the third stage uses not only $\hat{x}_2[n]$ but also $\hat{x}_1[n]$ and $y[n]$. Closer inspection of Fig. 9 shows that, because each stage has only a delay of D when the differentiator is replaced by an FIR filter, the DMC-RD has indeed a reduced total delay compared with the DMC.

To derive the second stage in Fig. 9, we recall that in the second DMC stage, $\hat{x}_1[n]$ runs through the first and second-order branch to reconstruct $e_1[n]$ and $e_2[n]$, respectively. The error analysis in (22) and (23) showed that the significant additional errors were introduced in the first-order branch, whereas those introduced in the second-order branch could be neglected. To reduce the delay, we therefore use $y[n]$ to reconstruct $e_2[n]$, rather than $\hat{x}_1[n]$. Clearly, we replace $\hat{e}_{22}[n]$ in (21) by

$$\tilde{e}_{22}[n] = \frac{1}{2}r_n^2 y''[n] \tag{38}$$

which can be approximated with (19) and neglecting terms of order $O(r_n^4)$ and higher by

$$\tilde{e}_{22}[n] \approx \frac{1}{2}r_n^2 x''[n] + \frac{1}{2}r_n^2 e_1''[n]. \tag{39}$$

Subtracting (20) and (38) from $y[n]$ cancels $e_1[n]$ and $e_2[n]$ and gives the reconstructed uniform sequence

$$\tilde{x}_2[n] = y[n] - \hat{e}_{21}[n] - \tilde{e}_{22}[n] \tag{40}$$

which corresponds to the output of the second stage. Fig. 9 depicts the second stage given by (20), (38) and (40). Comparing it with Fig. 7 shows that we could have obtained it by rewiring the second-order branch of the second DMC stage. Using (19), (22) and (39), we can approximate (40) by

$$\tilde{x}_2[n] \approx x[n] + r_n\left(r_n e_1'[n]\right)' - r_n e_2'[n] - \frac{1}{2}r_n^2 e_1''[n] + e_3[n]. \tag{41}$$

Comparing $\hat{x}_2[n]$ in (25) with (41) shows that the additional error $(1/2)r_n^2 e_1''[n]$ has been introduced. The simulation results in Section IX will show that this additional error slightly decreases the reconstruction performance of the DMC-RD compared with the DMC.

By a similar argument, we can derive the third stage in Fig. 9. Recall that in the third DMC stage, $\hat{x}_2[n]$ runs through the second and third-order branch to reconstruct $e_2[n]$ and $e_3[n]$, respectively. Because the additional errors introduced in these branches could be neglected, we use $\hat{x}_1[n]$ to reconstruct $e_2[n]$, and $y[n]$ to reconstruct $e_3[n]$. Clearly, we replace $\hat{e}_{32}[n]$ in (28) and $\hat{e}_{33}[n]$ in (29) by

$$\tilde{e}_{32}[n] = \frac{1}{2}r_n^2 \hat{x}_1''[n] \tag{42}$$

$$\tilde{e}_{33}[n] = \frac{1}{6}r_n^3 y'''[n] \tag{43}$$

respectively. Subtracting (42) and (43) together with $\hat{e}_{31}[n]$ in (27) from $y[n]$ gives the reconstructed uniform sequence

$$\tilde{x}_3[n] = y[n] - \hat{e}_{31}[n] - \tilde{e}_{32}[n] - \tilde{e}_{33}[n] \tag{44}$$

which corresponds to the output of the third stage. Fig. 9 depicts the third stage given by (27) and (42)–(44). Comparing it with Fig. 7 shows that we could have obtained it by rewiring the second and the third-order branch of the third DMC stage. Similar to the analysis in (41), it can be shown by approximating $\tilde{x}_3[n]$ that an additional error has been introduced, which again

decreases the reconstruction performance of the DMC-RD compared with the DMC.

Finally, because each stage in Fig. 9 has only a delay of D, the total delay of the DMC-RD with m stages is

$$D_m^{\mathrm{DMC-RD}} = mD, \qquad m = 1,2,3 \tag{45}$$

which is less than that of the DMC in (37). For the example $D = 16$ from before, the total delay with three stages is $D_3^{\mathrm{DMC-RD}} = 48$ which is only half of the total delay of the DMC.

VII. Performance Analysis of DMC

To determine the theoretical reconstruction performance of the DMC, we derive in this section the SNR at the output of each stage for a sinusoidal input signal. Although outlined for arbitrary M, we derive the SNR explicitly only for $M = 2$ and large M.

A. SNR for $M = 2$

We define the SNR at the output of the ith stage as

$$\mathrm{SNR_i} = 10\log_{10}\left(\frac{\int_{-\pi}^{\pi}\left|X(e^{j\omega})\right|^2 d\omega}{\int_{-\pi}^{\pi}\left|\bar{E}_i(e^{j\omega})\right|^2 d\omega}\right) \tag{46}$$

where the nominator represents the energy of the input sequence $x[n]$ with the corresponding discrete-time Fourier transform (DTFT) $X(e^{j\omega})$, and the denominator represents the energy of the remaining error $\bar{e}_i[n]$ with the corresponding DTFT $\bar{E}_i(e^{j\omega})$. Since the time errors are M-periodic, i.e., $r_n = r_{n+M}$, they can be represented by the discrete-time Fourier series [1]

$$r_n = \sum_{k=0}^{M-1} a_k e^{jk\frac{2\pi}{M}n}, \qquad n = 0,1,\ldots,M-1 \tag{47}$$

with Fourier series coefficients a_k.

With the period $M = 2$ and assuming r_n to be zero-mean, we obtain $a_0 = 0$ and $a_1 = r_0$, and therefore

$$r_n = r_0 e^{j\pi n}. \tag{48}$$

Using (48) and given a sampled sinusoidal input signal $x[n] = \sqrt{2}\sin(\omega_0 n)$, we show in Appendix A that the SNR at the output of the three DMC stages is given by

$$\mathrm{SNR}_1 = 10\log_{10}\left(\frac{1}{r_0^4\omega_0^2\left(\pi - \frac{1}{2}\omega_0\right)^2}\right) \tag{49}$$

$$\mathrm{SNR}_2 = 10\log_{10}\left(\frac{1}{r_0^6\omega_0^4\left(\pi - \frac{2}{3}\omega_0\right)^2}\right) \tag{50}$$

$$\mathrm{SNR}_3 = 10\log_{10}\left(\frac{1}{r_0^8\omega_0^4\left(\pi^2 - \frac{5}{3}\pi\omega_0 + \frac{5}{8}\omega_0^2\right)^2}\right) \tag{51}$$

for $0 < \omega_0 < \pi$. Note that, contrary to the assumption of zero-mean time errors r_n in this paper, an expression for SNR_1 was derived in [19] assuming $r_0 = 0$; this led to a more efficient polyphase implementation of the first stage since every second sampling instance is ideal.

B. SNR for Large M

In principle, we could derive the SNR for arbitrary M by finding the corresponding discrete-time Fourier series in (47) and following the derivation in Appendix A. But with increasing M, the derivation becomes tedious because of the increasing number of Fourier series coefficients a_k. For large M, though, the following consideration simplifies the derivation. The spectrum of an M-periodic nonuniformly sampled sinusoidal signal contains $M - 1$ spurious tones within the frequency range $[0, \pi)$. For small M, the magnitude of each tone depends heavily on the particular values of the time errors r_n [25]. As M increases, this dependence becomes less significant because the error power due to nonuniform sampling is distributed over an increasing number of spurious tones. Since this may be thought of as a noise floor introduced by nonuniform sampling, we use a stochastic analysis in the following. In particular, we replace the known time errors r_n by a wide-sense stationary and ergodic discrete-time random process. We assume that this random process has zero mean and the autocorrelation function

$$R_r[k] = E\{r_n r_{n+k}\} = \sigma_r^2\delta[k] \tag{52}$$

with the average power $R_r[0] = \sigma_r^2$. Similarly, denoting the autocorrelation function of $x[n]$ and $\bar{e}_i[n]$ as $R_x[k]$ and $R_{\bar{e}_i}[k]$, respectively, with the corresponding average power $R_x[0]$ and $R_{\bar{e}_i}[0]$, we define the SNR at the output of the ith stage as

$$\mathrm{SNR_i} = 10\log_{10}\left(\frac{R_x[0]}{R_{\bar{e}_i}[0]}\right). \tag{53}$$

Because we perform a stochastic analysis, we consider a sampled sinusoidal input signal of the form $x[n] = \sqrt{2}\sin(\omega_0 n + \theta)$. Assuming the random phase θ to be uniformly distributed in the interval $[0, 2\pi)$, the sinusoidal sequence $x[n]$ has the autocorrelation function

$$R_x[k] = E\{x[n]x[n+k]\} = \cos(\omega_0 k) \tag{54}$$

and the average power $R_x[0] = 1$. Given these assumptions, we show in Appendix B that the SNR at the output of the three DMC stages is given by

$$\mathrm{SNR}_1 = 10\log_{10}\left(\frac{1}{\sigma_r^4\omega_0^2\left(\frac{\pi^2}{3} + \frac{3}{4}\omega_0^2\right)}\right) \tag{55}$$

$$\mathrm{SNR}_2 = 10\log_{10}\left(\frac{1}{\sigma_r^6\omega_0^2\left(\frac{\pi^4}{9} + \frac{\pi^2}{6}\omega_0^2 + \frac{2}{3}\omega_0^4\right)}\right) \tag{56}$$

$$\mathrm{SNR}_3 = 10\log_{10}\left(\frac{1}{\sigma_r^8\omega_0^2\left(\frac{\pi^6}{27} + \frac{\pi^4}{18}\omega_0^2 + \frac{2\pi^2}{9}\omega_0^4 + \frac{35}{192}\omega_0^6\right)}\right) \tag{57}$$

for $0 < \omega_0 < \pi$. Based on the derivations in Appendix A and Appendix B, SNR expressions can also be obtained for the DMC-RD.

VIII. Implementation Issues

A practical implementation of the proposed reconstruction systems requires the design of a filter whose frequency response

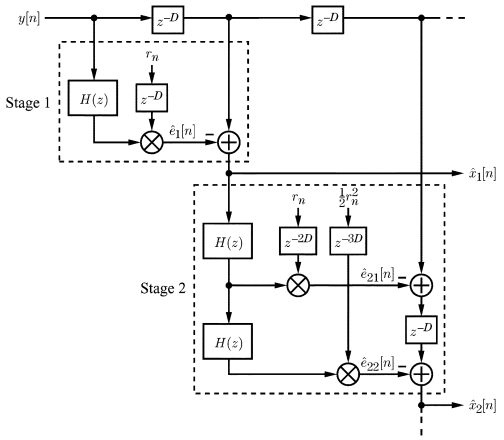

Fig. 10. Practical implementation of the DMC with two stages using a linear-phase FIR filter $H(z)$ with filter delay D.

approximates the frequency response of the ideal discrete-time differentiator $H_d(e^{j\omega})$ in (12). In this paper, we consider the design of a differentiator using a causal linear-phase FIR filter with frequency response $H(e^{j\omega})$ and filter delay D. The advantage of using this filter is that it can be easily designed in MATLAB and that its antisymmetric impulse response allows us to reduce the number of filter coefficients. Fig. 10 shows a practical implementation of the DMC with two stages using an FIR filter with z-transform $H(z)$. Due to the filter delay, the time errors in the reconstruction branches of each stage are also delayed. Consider, for example, the second stage in the figure. To generate $\hat{e}_{21}[n]$, the time errors r_n in the first-order branch are delayed by $2D$ because $y[n]$ runs through two FIR filters before it is multiplied by r_n in this branch. Consequently, $y[n]$ is also delayed by $2D$ before $\hat{e}_{21}[n]$ can be subtracted. Similar delays are used when implementing the DMC-RD.

The filter delay also becomes crucial for choosing the type of linear-phase FIR filter. Because the ideal differentiator has an antisymmetric impulse response, the FIR filter realizing the differentiator can only be of type III or IV [1]. In general, an FIR filter of type IV has a delay of an integer (depending on the filter order) plus one-half; this would require delaying the time errors by one-half, too, which could only be done by interpolating them. Therefore, we use an FIR filter of type III, which has an odd number of filter coefficients P and an integer delay $D = (P-1)/2$ [1]. Moreover, because the frequency response of this filter has a zero at π, the designed differentiator shows an additional low-pass characteristic and requires a cut-off frequency ω_c for the design. The drawback is that this low-pass characteristic introduces a certain amount of oversampling. Although a larger ω_c for the design reduces oversampling, the number of filter coefficients, and thus the overall complexity, may increase considerably. On balance, the antisymmetric impulse response of the filter allows us to additionally halve the number of filter coefficients [1].

IX. Simulation Results

This section presents simulation results that illustrate the design and performance of the DMC and the DMC-RD with three stages. For the simulations, we designed an FIR differentiator using the MATLAB function `firpm`, which uses the Parks-McClellan optimal equiripple design algorithm [1]. To evaluate the overall reconstruction performance, we computed the SNR at the output of each stage over $N = 8192$ samples. For the ith stage, the SNR was computed by

$$\mathrm{SNR_i} = 10\log_{10}\left(\frac{\sum_{n=0}^{N-1}|x[n]|^2}{\sum_{n=0}^{N-1}|o_i[n]-x[n-D_i]|^2}\right) \qquad (58)$$

where the output sequence $o_i[n] = \hat{x}_i[n]$ for the DMC and $o_i[n] = \tilde{x}_i[n]$ for the DMC-RD, for $i = 2, 3$, and $o_1[n] = \hat{x}_1[n]$ for both systems. The delay D_i was computed by (37) for the DMC and by (45) for the DMC-RD. Because there are i filters in the ith stage of each system, the total number of filter coefficients for both systems with m stages is

$$P_m = \sum_{i=1}^{m} iP = \frac{1}{2}m(m+1)P, \qquad m = 1, 2, 3. \qquad (59)$$

Furthermore, the time errors r_n used in the simulations were either predefined or a sequence of independent and identically distributed Gaussian random numbers with zero mean and standard deviation σ_r.

To confirm the theoretical SNR derived in Section VII-A for the DMC and $M = 2$, we sampled a sinusoidal signal nonuniformly with time errors $r_1 = -r_0 = 0.005$ while increasing its frequency from 0 to the Nyquist frequency $\Omega_s/2$. Fig. 11(a) shows that the computed SNR at the output of the three stages matches the theoretical SNR given by (49), (50) and (51), confirming also the discussion in Section V that the reconstruction performance of the ith stage is only determined by errors up to order $O(r_n^{i+1})$. The deviation for frequencies close to zero and close to the Nyquist frequency is due to the low-pass characteristic of the designed FIR differentiator, as discussed in Section VIII. In particular, a two-periodic nonuniformly sampled sinusoidal signal with frequency ω_0 has a spurious tone at $\pi - \omega_0$. For ω_0 close to zero, this tone falls into the cut-off region of the FIR differentiator, causing the error power to decrease and thus the SNR to increase. For ω_0 close to the Nyquist frequency, the tone falls directly into the cut-off region, causing the signal power to decrease and thus also the SNR; this explains the need for an oversampled input signal. However, the figure also shows that oversampling can be reduced by designing a differentiator with a higher cut-off frequency ω_c and a sufficiently large number of filter coefficients P, but at the cost of an increased overall complexity. Moreover, for fixed filter design parameters (say, for $\omega_c = 0.8\pi$ and $P = 51$), oversampling increases with each additional stage because the chain of differentiators in each stage decreases the overall cut-off frequency. Finally, we can directly compare this figure with Fig. 6 in our previous work [19]. In that paper, we assumed $r_0 = 0$ and $r_1 = 0.01$ (half of the sampling instances are ideal), which corresponds to time-shifting the time errors assumed in Fig. 11(a) by 0.005. The comparison shows that assuming half of the sampling instances to be ideal gives an improved SNR for frequencies close to the Nyquist frequency, besides the advantage of effectively reducing the number of filter taps by two.

To confirm the theoretical SNR derived in Section VII-B for large M, the same simulation was run with $M = 8192$ time errors $(\sigma_r = 0.01)$. Because the SNR was computed over 8192 samples, this simulation demonstrates the reconstruction performance for the general nonuniform sampling case. Fig. 11(b) shows that the computed SNR at the output of the three stages matches the theoretical SNR given by (55)–(57) up to some dB.

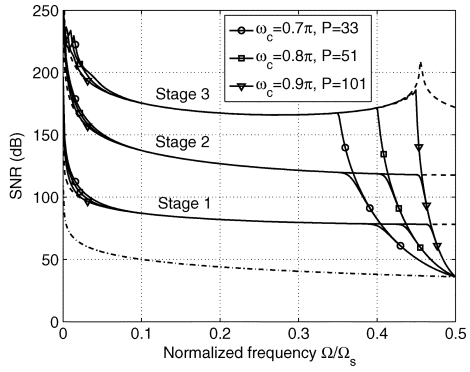

(a)

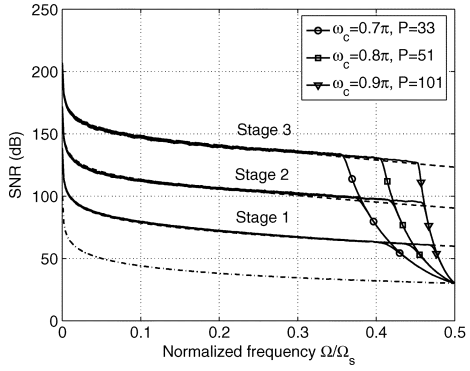

(b)

Fig. 11. SNR versus normalized frequency for reconstructing a nonuniformly sampled sinusoidal signal: Computed SNR before reconstruction (dash-dotted), theoretical SNR (dashed) and computed SNR after reconstruction using the DMC for different filter design parameters ω_c and P (solid). (a) Time errors: $M = 2, r_n = \{-0.005, 0.005\}$. (b) Time errors: $M = 8192, \sigma_r = 0.01$.

The deviation is due to the cross-terms that were neglected in the SNR derivation in Appendix B.

In Fig. 11, a large number of filter coefficients was chosen in order to confirm the theoretical SNR of each stage. To illustrate the implementation complexity in a practical case, we chose an example from [18], where $M = 4$, the filter cut-off frequency $\omega_c = 0.8\pi$ and the magnitude of the time errors is less than 0.02. Using the DMC with two stages for the reconstruction, we performed the same simulation as in Fig. 11 but for different time errors, three of which are shown in Fig. 12. An SNR of 80 dB over the frequency range $[0, 0.8\pi]$ as design goal is achieved with an FIR differentiator designed with $P = 23$ filter coefficients. With the total number of filter coefficients $P_2 = 69$ computed by (59), an implementation of the system using transposed direct-form FIR structures requires 33 fixed multipliers for the three FIR filters and three general multipliers for the time-varying multipliers. We emphasize that, because of the different design specifications, it is difficult to directly compare the resulting implementation complexity to that of the polynomial impulse response time-varying FIR filters in [18]. For the given example, the filters in [18] were designed in the minimax sense, which is a much stricter design goal because for every sampling instance, the error after reconstruction is guaranteed to be less than a specified one.

To determine the number of filter coefficients required to achieve a certain SNR, we sampled a noise signal, bandlimited to the filter cut-off frequency ω_c, nonuniformly with $M = 16$ time errors ($\sigma_r = 0.01$) and reconstructed it using the DMC

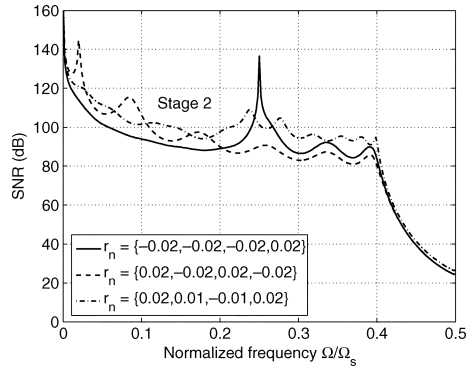

Fig. 12. SNR versus normalized frequency for reconstructing a nonuniformly sampled sinusoidal signal: Computed SNR after reconstruction using the DMC for different time errors ($M = 4$). Filter design parameters: $\omega_c = 0.8\pi$, $P = 23$.

and the DMC-RD. Fig. 13 compares the SNR of the second and third stage of both systems for different filter cut-off frequencies ω_c (a similar plot showing the SNR of the first stage for $M = 2$ can be found in [19]). Each data point represents the SNR for an FIR differentiator designed with P filter taps, with the total number of coefficients computed by (59). It can be seen that with increasing P, the SNR at the output of each stage increases up to a maximal value where the differentiator is sufficiently well designed and the SNR is only limited by the remaining error of each stage. As illustrated in Fig. 13(a) for $\omega_c = 0.8\pi$, the second stage of the DMC achieves an SNR of 95 dB with a total number of 63 filter taps. To get the same SNR for $\omega_c = 0.9\pi$ requires 123 filter coefficients, i.e., about twice as many. Although Fig. 13(b) shows that the third stage achieves an SNR of up to about 130 dB, the number of filter coefficients increases considerably, especially for small oversampling. The two figures also confirm that the DMC-RD performs slightly worse than the DMC, as discussed in Section VI.

The dependence of the reconstruction performance on the magnitude of the time errors r_n is illustrated in Fig. 14. We sampled a noise signal, bandlimited to the filter cut-off frequency ω_c, nonuniformly with $M = 2$ and $M = 8192$ time errors and used the DMC for reconstruction. We generated 20 uniformly distributed random numbers in the interval [0.001,0.1], using them as σ_r to produce time errors with varying magnitude. The figure shows the SNR after reconstruction as a function of the SNR before reconstruction. Each data point corresponds to one of the 20 values, and the lines interpolating the data points indicate the SNR tendency. Since time errors large (small) in magnitude give a small (large) SNR before reconstruction, it can be seen that the SNR after reconstruction decreases with increasing magnitude of the time errors. Reconstruction eventually fails once the magnitude of the time errors exceeds a maximum value where the lines in the figure intersect; this makes our assumption of time errors less than some tenth necessary, similar to the polynomial impulse response time-varying FIR filters [17]. The figure also illustrates the influence of the filter design on the reconstruction performance. The SNR at the output of the third stage increases roughly linearly with decreasing magnitude of the time errors or, equivalently, with increasing SNR before reconstruction. This SNR increase at the output flattens as the magnitude of the time errors becomes too small, indicating

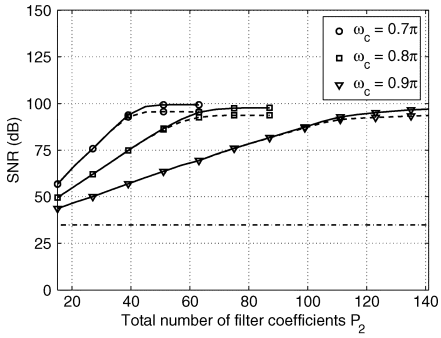

(a)

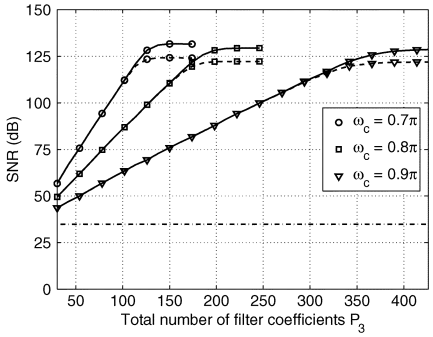

(b)

Fig. 13. SNR versus total number of filter coefficients for reconstructing a nonuniformly sampled noise signal, bandlimited to different filter cut-off frequencies ω_c: Computed SNR before reconstruction (dash-dotted) and after reconstruction using the DMC (solid) and the DMC-RD (dashed). Time errors: $M = 16$, $\sigma_r = 0.01$. (a) Output of stage 2. (b) Output of stage 3.

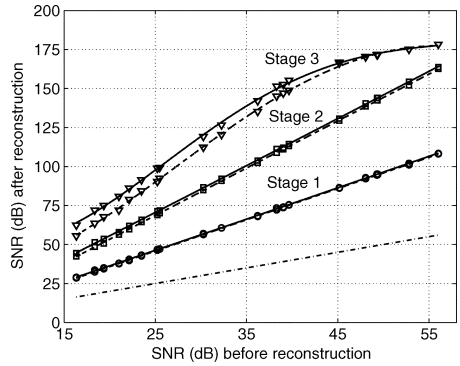

Fig. 14. SNR after versus SNR before reconstructing a nonuniformly sampled noise signal, bandlimited to the filter cut-off frequency ω_c: Computed SNR before reconstruction (dash-dotted) and after reconstruction using the DMC. Time errors: $M = 2$ (solid) and $M = 8192$ (dashed); 20 values for σ_r, given by uniformly distributed random numbers in the interval [0.001,0.1]. Filter design parameters: $\omega_c = 0.8\pi$, $P = 41$.

that more filter coefficients are needed to design the differentiator when the SNR before reconstruction is large.

The oversampling performance of the DMC and the DMC-RD is compared in Fig. 15. We sampled a bandlimited noise signal nonuniformly with $M = 64$ time errors $(\sigma_r = 0.01)$ while increasing its bandwidth from 0 to the Nyquist frequency $\Omega_s/2$ (the maximum bandwidth). The figure illustrates that oversampling increases with each additional stage. More specifically, the first stage improves the SNR for a noise signal bandlimited up to 0.9 times the Nyquist frequency, despite a filter cut-off frequency ω_c of only 0.8π. Although oversampling reduces to 0.8 with three stages, the SNR at the

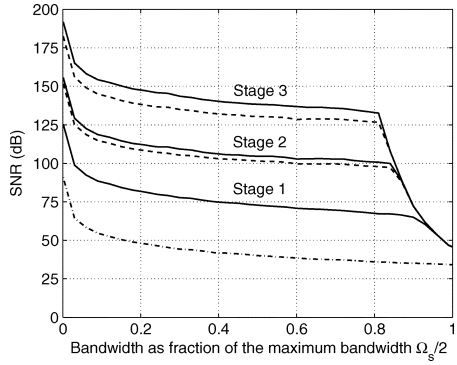

Fig. 15. SNR versus normalized bandwidth for reconstructing a nonuniformly sampled bandlimited noise signal: Computed SNR before reconstruction (dash-dotted) and after reconstruction using the DMC (solid) and the DMC-RD (dashed). Time errors: $M = 64$, $\sigma_r = 0.01$. Filter design parameters: $\omega_c = 0.8\pi$, $P = 41$.

output of the third stage is significant. Similar to Fig. 13, this figure also shows that the DMC-RD performs slightly worse than the DMC.

X. Conclusion

This paper has introduced the DMC, a novel system for reconstructing a bandlimited signal from its nonuniform samples. The system improves the reconstruction performance by a cascade of reconstruction stages, each consisting only of linear-phase FIR filters and time-varying multipliers. The main advantage is that, because the FIR filters are designed as differentiators, the system can be used for the general nonuniform sampling case and is not restricted to periodic nonuniform sampling. Moreover, once the FIR differentiators have been designed, they are implemented with fixed filter coefficients such that implementation costs are reduced. When the nonuniform sampling pattern changes over time, no filter redesign is required and only a few general multipliers need to be adapted; this is advantageous, for example, in TI-ADCs where temperature and aging effects cause the timing mismatches among the ADCs to vary during operation.

Several issues in the design and implementation of the proposed reconstruction system need further investigations. A major advantage of the system is the design of a simple FIR differentiator, even for the general nonuniform sampling case. However, apart from the cases $M = 2$ and large M, where we have found analytic SNR expressions, there is the need for a systematic technique to choose the number of filter coefficients in the design such that the SNR at the system output achieves a specified value. The selection can be formulated as an optimization problem, but with a significantly reduced complexity compared to [18] since the filters and the structure are fixed. Also, different filter design methods, such as those based on least-squares error minimization, and a different number of filter coefficients for each differentiator in each stage might be compared in terms of the resulting reconstruction performance. Furthermore, a potential issue in an implementation of the proposed reconstruction system is the effect of quantization due to the finite register lengths. In particular, if the magnitude of the time errors r_n decreases, the time-varying multipliers $r_n^l/l!$ in each stage become even smaller and, if not quantized with a sufficient number of bits, impair the reconstruction performance.

APPENDIX A
DERIVATION OF SNR FOR $M = 2$

A. SNR of the First Stage in (49)

We begin by replacing each error term in (33) by its explicit expression in (11). Then, substituting (48) for r_n gives

$$\bar{e}_1[n] \approx \frac{1}{2} r_0^2 x''[n] - r_0^2 e^{j\pi n} \left(e^{j\pi n} x'[n]\right)'. \tag{60}$$

By computing the squared magnitude of the DTFT of (60), the energy density spectrum is found to be

$$\left|\bar{E}_1(e^{j\omega})\right|^2 = r_0^4 \left| H_d(e^{j\omega}) \left[\frac{1}{2} H_d(e^{j\omega}) - H_d\left(e^{j(\omega-\pi)}\right)\right]\right|^2 \times \left|X(e^{j\omega})\right|^2. \tag{61}$$

Because the first term of this product is an even function, it is sufficient to consider only positive frequencies. With (12), we can thus write

$$\left| H_d(e^{j\omega}) \left[\frac{1}{2} H_d(e^{j\omega}) - H_d\left(e^{j(\omega-\pi)}\right)\right]\right|^2 = \omega^2 \left(\pi - \frac{1}{2}\omega\right)^2 \tag{62}$$

for $0 < \omega < \pi$. Substituting (62) and the DTFT of the sinusoidal sequence $x[n] = \sqrt{2}\sin(\omega_0 n)$ into (61), and integrating over 2π, we get

$$\int_{-\pi}^{\pi} \left|\bar{E}_1(e^{j\omega})\right|^2 d\omega = r_0^4 \omega_0^2 \left(\pi - \frac{1}{2}\omega_0\right)^2 \tag{63}$$

for $0 < \omega_0 < \pi$, and thus the SNR of the first stage in (49).

B. SNR of the Second Stage in (50)

Similar to the first stage, replacing each error term in (34) by its explicit expression in (11) and inserting (48) gives after simplification

$$\bar{e}_2[n] \approx -\frac{1}{3} r_0^3 e^{j\pi n} x'''[n] + r_0^3 e^{j\pi n} \left(e^{j\pi n} \left(e^{j\pi n} x'[n]\right)'\right)'. \tag{64}$$

Computing the squared magnitude of the DTFT of (64) gives the energy density spectrum

$$\left|\bar{E}_2(e^{j\omega})\right|^2 = r_0^6 \left| H_d^2\left(e^{j(\omega-\pi)}\right) \times \left[\frac{1}{3} H_d\left(e^{j(\omega-\pi)}\right) - H_d(e^{j\omega})\right]\right|^2 \left|X\left(e^{j(\omega-\pi)}\right)\right|^2 \tag{65}$$

where, for $0 < \omega < \pi$ and using (12), the first term of this product can be written as

$$\left| H_d^2\left(e^{j(\omega-\pi)}\right) \left[\frac{1}{3} H_d\left(e^{j(\omega-\pi)}\right) - H_d(e^{j\omega})\right]\right|^2 = (\pi - \omega)^4 \left(\frac{1}{3}\pi + \frac{2}{3}\omega\right)^2. \tag{66}$$

Substituting (66) and the DTFT of the sinusoidal sequence into (65), and integrating over 2π, we get

$$\int_{-\pi}^{\pi} \left|\bar{E}_2(e^{j\omega})\right|^2 d\omega = r_0^6 \omega_0^4 \left(\pi - \frac{2}{3}\omega_0\right)^2 \tag{67}$$

for $0 < \omega_0 < \pi$, and thus the SNR of the second stage in (50). The SNR derivation of the third stage in (51) will be omitted because it is similar to that of the first and second stage.

APPENDIX B
DERIVATION OF SNR FOR LARGE M

We begin with the definition of the SNR in (53). Since $R_x[0] = 1$ by assumption, we only need to find $R_{\bar{e}_i}[0]$ to obtain the SNR of the ith stage. Using (36) and neglecting the cross term to simplify the derivation yields

$$\begin{aligned} R_{\bar{e}_i}[0] &= E\left\{|\bar{e}_i[n]|^2\right\} \approx E\left\{|e_{i+1}[n]|^2\right\} + E\left\{\left|r_n \bar{e}'_{i-1}[n]\right|^2\right\} \\ &= R_{e_{i+1}}[0] + R_{r\bar{e}'_{i-1}}[0]. \end{aligned} \tag{68}$$

Approximating the autocorrelation function of $\bar{e}_i[n]$ by

$$R_{\bar{e}_i}[k] \approx R_{e_{i+1}}[k] + R_{r\bar{e}'_{i-1}}[k] \tag{69}$$

we obtain (68) from (69) with $k = 0$. In the following, we derive an expression for each term in (69).

1) $R_{e_{i+1}}[k]$: Setting $i = l - 1$, the autocorrelation function of $e_l[n]$ in (11) is

$$R_{e_l}[k] = \frac{1}{(l!)^2} E\left\{r_n^l r_{n+k}^l x^{(l)}[n] x^{(l)}[n+k]\right\}. \tag{70}$$

Because the time errors r_n and the random phase θ of the sinusoidal sequence $x[n] = \sqrt{2}\sin(\omega_0 n + \theta)$ are independent, r_n^l and $x^{(l)}[n]$ are independent, too, and we can write (70) as

$$\begin{aligned} R_{e_l}[k] &= \frac{1}{(l!)^2} E\left\{r_n^l r_{n+k}^l\right\} E\left\{x^{(l)}[n] x^{(l)}[n+k]\right\} \\ &= \frac{1}{(l!)^2} R_{r^l}[k] \omega_0^{2l} \cos(\omega_0 k) \end{aligned} \tag{71}$$

where we have used $R_{x^{(l)}}[k] = \omega_0^{2l}\cos(\omega_0 k)$, the autocorrelation function of the lth derivative of $x[n]$. To find the joint moment function $R_{r^l}[k]$, consider r_n for a fixed n. Since for each k, the resulting random variables r_n and r_{n+k} are jointly Gaussian with zero mean, their joint moment generating function is [26]

$$\phi_{r_n, r_{n+k}}(s_1, s_2) = e^{\frac{1}{2}\left(R_r[0]s_1^2 + 2s_1 s_2 R_r[k] + R_r[0]s_2^2\right)} \tag{72}$$

where s_1 and s_2 are real variables. From this equation, $R_{r^l}[k]$ is obtained by [26]

$$R_{r^l}[k] = \frac{\partial^{2l}}{\partial^l s_1 \partial^l s_2} \phi_{r_n, r_{n+k}}(s_1, s_2)\big|_{s_1 = s_2 = 0}. \tag{73}$$

2) $R_{r\bar{e}'_{i-1}}[k]$: To compute the autocorrelation function of $r_n\bar{e}'_{i-1}[n]$, we need the joint probability density function of r_n and $\bar{e}'_{i-1}[n]$ because the two sequences are not independent ($\bar{e}'_{i-1}[n]$ also depends on r_n). However, simulation results have shown that we can approximately write

$$\begin{aligned} R_{r\bar{e}'_{i-1}}[k] &\approx E\{r_n r_{n+k}\} E\left\{\bar{e}'_{i-1}[n]\bar{e}'_{i-1}[n+k]\right\} \\ &= \sigma_r^2 R_{\bar{e}'_{i-1}}[0]\delta[k] \end{aligned} \tag{74}$$

where we have used $R_r[k] = \sigma_r^2\delta[k]$, and $z[k]\delta[k] = z[0]\delta[k]$ for any sequence $z[k]$. Because $R_{\bar{e}'_{i-1}}[k]$ is the autocorrelation function of the differentiator output when the input is $\bar{e}_{i-1}[n]$ (see Fig. 8), we have the relation [26]

$$R_{\bar{e}'_{i-1}}[k] = g[k] * R_{\bar{e}_{i-1}}[k] \tag{75}$$

where

$$g[k] := h_d[k] * h_d[-k] = \frac{1}{2\pi}\int_{-\pi}^{\pi} \left|H_d(e^{j\omega})\right|^2 e^{j\omega k} d\omega. \tag{76}$$

3) $R_{\bar{e}_i}[k]$: Substituting (71) with $l = i+1$ and (74) into (69) gives

$$R_{\bar{e}_i}[k] \approx \frac{1}{((i+1)!)^2} R_{r^{i+1}}[k]\omega_0^{2(i+1)}\cos(\omega_0 k) + \sigma_r^2 R_{\bar{e}'_{i-1}}[0]\delta[k] \tag{77}$$

where $R_{\bar{e}'_{i-1}}[0]$ is obtained by evaluating the convolution in (75) at $k = 0$. Equation (77) gives an approximate recursive relation between $R_{\bar{e}_i}[k]$ and $R_{\bar{e}_{i-1}}[k]$, the autocorrelation function of the remaining error of the ith stage and the $(i-1)$th stage, respectively. With this equation and the definition of the SNR in (53), we now derive the SNR of each stage by recursively computing $R_{\bar{e}_i}[k]$ (beginning with the first stage) and evaluating the resulting expression at $k = 0$.

A. SNR of the First Stage in (55)

Setting $i = 1$ in (77), we get

$$R_{\bar{e}_1}[k] \approx \frac{1}{4} R_{r^2}[k]\omega_0^4\cos(\omega_0 k) + \sigma_r^2 R_{\bar{e}'_0}[0]\delta[k] \tag{78}$$

where $R_{r^2}[k]$ is obtained from (72) and (73) with $l = 2$ as

$$R_{r^2}[k] = 2R_r^2[k] + R_r^2[0] = \sigma_r^4\left(2\delta[k] + 1\right). \tag{79}$$

To find $R_{\bar{e}'_0}[0]$ in (78), we compute $R_{\bar{e}'_0}[k]$ and evaluate it at lag zero. Since $R_{\bar{e}_0}[0] = R_{e_1}[0]$, we get from (71) with $l = 1$

$$R_{e_1}[k] = R_r[k]\omega_0^2\cos(\omega_0 k) = \sigma_r^2\omega_0^2\delta[k] \tag{80}$$

and from (75) with $i = 1$

$$R_{\bar{e}'_0}[k] = g[k] * R_{e_1}[k] = \sigma_r^2\omega_0^2 g[k]. \tag{81}$$

To evaluate (81) at zero, we replace $H_d(e^{j\omega})$ in (76) by (12), set $k = 0$ and integrate. This gives

$$g[0] = \frac{\pi^2}{3} \tag{82}$$

and hence for (81) at lag zero $R_{\bar{e}'_0}[0] = \sigma_r^2\omega_0^2\pi^2/3$. Finally, inserting this term and (79) into (78) yields

$$R_{\bar{e}_1}[k] \approx \sigma_r^4\omega_0^2\left[\left(\frac{\pi^2}{3} + \frac{1}{2}\omega_0^2\right)\delta[k] + \frac{1}{4}\omega_0^2\cos(\omega_0 k)\right] \tag{83}$$

with the resulting average power

$$R_{\bar{e}_1}[0] \approx \sigma_r^4\omega_0^2\left(\frac{\pi^2}{3} + \frac{3}{4}\omega_0^2\right) \tag{84}$$

and thus the SNR of the first stage in (55).

B. SNR of the Second Stage in (56)

Setting $i = 2$ in (77), we get

$$R_{\bar{e}_2}[k] \approx \frac{1}{36} R_{r^3}[k]\omega_0^6\cos(\omega_0 k) + \sigma_r^2 R_{\bar{e}'_1}[0]\delta[k] \tag{85}$$

where $R_{r^3}[k]$ is obtained from (72) and (73) with $l = 3$ as

$$R_{r^3}[k] = 9R_r^2[0]R_r[k] + 6R_r^3[k] = 15\sigma_r^6\delta[k]. \tag{86}$$

To find $R_{\bar{e}'_1}[0]$ in (85), we compute $R_{\bar{e}'_1}[k]$ and evaluate it at lag zero. Setting $i = 2$ in (75) and inserting (83) gives

$$\begin{aligned} R_{\bar{e}'_1}[k] &= g[k] * R_{\bar{e}_1}[k] \\ &\approx \sigma_r^4\omega_0^2\left[\left(\frac{\pi^2}{3} + \frac{1}{2}\omega_0^2\right) g[k] \right. \\ &\qquad \left. + \frac{1}{4}\omega_0^2 g[k] * \cos(\omega_0 k)\right]. \end{aligned} \tag{87}$$

To evaluate this equation at zero, we express the convolution with (76) and the DTFT of $\cos(\omega_0 k)$ as

$$g[k] * \cos(\omega_0 k) = \int_0^{\pi} \left|H_d(e^{j\omega})\right|^2 \delta(\omega - \omega_0) e^{j\omega k} d\omega. \tag{88}$$

Replacing $H_d(e^{j\omega})$ by (12), setting $k = 0$ and integrating gives ω_0^2, and hence for (87) with (82) at lag zero

$$R_{\bar{e}'_1}[0] \approx \sigma_r^4\omega_0^2\left(\frac{\pi^4}{9} + \frac{\pi^2}{6}\omega_0^2 + \frac{1}{4}\omega_0^4\right). \tag{89}$$

Finally, inserting (86) and (89) into (85) yields

$$R_{\bar{e}_2}[k] \approx \sigma_r^6\omega_0^2\left(\frac{\pi^4}{9} + \frac{\pi^2}{6}\omega_0^2 + \frac{2}{3}\omega_0^4\right)\delta[k] \tag{90}$$

and thus with $k = 0$ the SNR of the second stage in (56).

C. SNR of the Third Stage in (57)

Setting $i = 3$ in (77), we get

$$R_{\bar{e}_3}[k] \approx \frac{1}{576} R_{r^4}[k]\omega_0^8 \cos(\omega_0 k) + \sigma_r^2 R_{\bar{e}_2'}[0]\delta[k] \qquad (91)$$

where $R_{r^4}[k]$ is obtained from (72) and (73) with $l = 4$ as

$$\begin{aligned} R_{r^4}[k] &= 72R_r^2[0]R_r^2[k] + 9R_r^4[0] + 24R_r^4[k] \\ &= \sigma_r^8 \left(96\delta[k] + 9\right). \end{aligned} \qquad (92)$$

Following the derivation of the SNR of the first and second stage, we obtain $R_{\bar{e}_2'}[k] = g[k] * R_{\bar{e}_2}[k]$ from (75) with $i = 3$, and with (82) and (90) at lag zero

$$R_{\bar{e}_2'}[0] \approx \sigma_r^6 \omega_0^2 \left(\frac{\pi^6}{27} + \frac{\pi^4}{18}\omega_0^2 + \frac{2\pi^2}{9}\omega_0^4\right). \qquad (93)$$

Finally, inserting (92) and (93) into (91) gives an expression for $R_{\bar{e}_3}[k]$ with the resulting average power

$$R_{\bar{e}_3}[0] \approx \sigma_r^8 \omega_0^2 \left(\frac{\pi^6}{27} + \frac{\pi^4}{18}\omega_0^2 + \frac{2\pi^2}{9}\omega_0^4 + \frac{35}{192}\omega_0^6\right) \qquad (94)$$

and thus the SNR of the third stage in (57).

REFERENCES

[1] A. V. Oppenheim, R. W. Schafer, and J. R. Buck, *Discrete-Time Signal Processing*. Upper Saddle River, NJ: Prentice-Hall, 1999.

[2] *Nonuniform Sampling: Theory and Practice*, F. A. Marvasti, Ed. Reading, MA: Kluwer Academic, 2001.

[3] F. Beutler, "Error free recovery of signals from irregularly spaced samples," *SIAM Rev.*, vol. 8, no. 3, pp. 328–335, Jul. 1966.

[4] J. L. Yen, "On nonuniform sampling of bandwidth-limited signals," *IRE Trans. Circuit Theory*, vol. CT-3, no. 4, pp. 251–257, Dec. 1956.

[5] H. Choi and D. C. Munson, "Analysis and design of minimax-optimal interpolators," *IEEE Trans. Signal Process.*, vol. 46, no. 6, pp. 1571–1579, Jun. 1998.

[6] R. G. Wiley, "Recovery of bandlimited signals from unequally spaced samples," *IEEE Trans. Commun.*, vol. COM-26, no. 1, pp. 135–137, Jan. 1978.

[7] H. Johansson and P. Löwenborg, "Reconstruction of nonuniformly sampled bandlimited signals by means of time-varying discrete-time FIR filters," *EURASIP J. Appl. Signal Process.*, vol. 2006, pp. 1–18, 2006, DOI 10.1155/ASP/2006/64185, 64185.

[8] Y. C. Eldar and A. V. Oppenheim, "Filterbank reconstruction of bandlimited signals from nonuniform and generalized samples," *IEEE Trans. Signal Process.*, vol. 48, no. 10, pp. 2864–2875, Oct. 2000.

[9] R. S. Prendergast, B. C. Levy, and P. J. Hurst, "Reconstruction of bandlimited periodic nonuniformly sampled signals through multirate filter banks," *IEEE Trans. Circuits Syst. I, Reg. Papers*, vol. 51, no. 8, pp. 1612–1622, Aug. 2004.

[10] W. Namgoong, "Finite-length synthesis filters for non-uniformly time-interleaved analog-to-digital converter," in *Proc. IEEE Int. Symp. Circuits Syst.*, May 2002, vol. 4, pp. 815–818.

[11] W. C. Black, Jr. and D. A. Hodges, "Time-interleaved converter arrays," *IEEE J. Solid-State Circuits*, vol. SC-15, no. 6, pp. 1022–1029, Dec. 1980.

[12] S. Huang and B. C. Levy, "Adaptive blind calibration of timing offset and gain mismatch for two-channel time-interleaved ADCs," *IEEE Trans. Circuits Syst. I, Reg. Papers*, vol. 53, no. 6, pp. 1278–1288, Jun. 2006.

[13] S. Huang and B. Levy, "Blind calibration of timing offsets for four-channel timeinterleaved ADCs," *IEEE Trans. Circuits Syst. I, Exp. Briefs*, vol. 54, no. 4, pp. 863–876, Apr. 2007.

[14] V. Ferragina, A. Fornasari, U. Gatti, P. Malcovati, and F. Maloberti, "Gain and offset mismatch calibration in time-interleaved multipath A/D sigma-delta modulators," *IEEE Trans. Circuits Syst. II, Exp. Briefs*, vol. 51, no. 12, pp. 2365–2373, Dec. 2004.

[15] H. Johansson and P. Löwenborg, "Reconstruction of nonuniformly sampled bandlimited signals by means of digital fractional delay filters," *IEEE Trans. Signal Process.*, vol. 50, no. 11, pp. 2757–2767, Nov. 2002.

[16] H. Johansson, P. Löwenborg, and K. Vengattaramane, "Reconstruction of two-periodic nonuniformly sampled signals using polynomial impulse response time-varying FIR filters," in *Proc. IEEE Int. Symp. Circuits Syst.*, May 2006, pp. 2993–2996.

[17] H. Johansson, P. Löwenborg, and K. Vengattaramane, "Least-squares and minimax design of polynomial impulse response FIR filters for reconstruction of two-periodic nonuniformly sampled signals," *IEEE Trans. Circuits Syst. I, Reg. Papers*, vol. 54, no. 4, pp. 877–888, Apr. 2007.

[18] H. Johansson, P. Löwenborg, and K. Vengattaramane, "Reconstruction of M-periodic nonuniformly sampled signals using multivariate impulse response time-varying FIR filters," in *Proc. XII Eur. Signal Process. Conf.*, Sep. 2006.

[19] S. Tertinek and C. Vogel, "Reconstruction of two-periodic nonuniformly sampled bandlimited signals using a discrete-time differentiator and a time-varying multiplier," *IEEE Trans. Circuits Syst. II, Exp. Briefs*, vol. 54, no. 7, pp. 616–620, Jul. 2007.

[20] M. Seo, M. J. W. Rodwell, and U. Madhow, "Comprehensive digital correction of mismatch errors for a 400-Msamples/s 80-dB SFDR time-interleaved analog-to-digital converter," *IEEE Trans. Microw. Theory Tech.*, vol. 53, no. 3, pp. 1072–1082, Mar. 2005.

[21] W. Rudin, *Principles of Mathematical Analysis*. New York: McGraw-Hill Publishing Co., 1976.

[22] C. W. Farrow, "A continuously variable digital delay element," in *Proc. IEEE Int. Symp. Circuits Syst.*, Espoo, Finland, Jun. 1988, vol. 3, pp. 2641–2645.

[23] S.-C. Pei and C.-C. Tseng, "An efficient design of a variable fractional delay filter using a first-order differentiator," *IEEE Signal Process. Lett.*, vol. 10, no. 10, pp. 307–310, Oct. 2003.

[24] M. J. Narasimha, A. Ignjatovic, and P. P. Vaidyanathan, "Chromatic derivative filter banks," *IEEE Signal Process. Lett.*, vol. 9, no. 7, pp. 215–216, Jul. 2002.

[25] Y.-C. Jenq, "Digital spectra of nonuniformly sampled signals: Fundamentals and high-speed waveform digitizers," *IEEE Trans. Instrum. Meas.*, vol. 37, no. 2, pp. 245–251, Jun. 1988.

[26] A. Papoulis and U. Pillai, *Probability, Random Variables and Stochastic Processes*, 4th ed. New York: McGraw-Hill, 2002.

Stefan Tertinek received the Dipl.-Ing. degree in electrical engineering from Graz University of Technology, Graz, Austria, in 2007. He is currently working toward the Ph.D. degree in the Circuits and Systems Group at University College Dublin, Ireland.

His research interests include the nonlinear analysis of digital phase-locked loops.

Christian Vogel (S'02–M'06) received the Dipl.-Ing. degree in telematikand the Dr. techn. degree in electrical and information engineering from Graz University of Technology, Graz, Austria, in 2001 and 2005, respectively.

Since 2008, he has been a Postdoctoral Researcher at the Signal and Information Processing Laboratory at ETH Zurich, Switzerland. His research interests include the design and theory of digital, analog, and mixed-signal processing systems with special emphasis on communication systems and digital enhancement techniques for analog signal processing systems.